~~SECRET~~

Copy
RM E56D13a

5

Copy 2

NACA RM E56D13a

CLASSIFICATION CHANGED

To UNCLASSIFIED

~~NACA~~

By authority of NASA Class. Change Notices, Issue no. 7, Sept. 15, 1964. NASA-10-5-64.

RESEARCH MEMORANDUM

TESTS WITH HYDROGEN FUEL IN A SIMULATED AFTERBURNER

By W. R. Kerslake and E. E. Dangle

Lewis Flight Propulsion Laboratory
Cleveland, Ohio

CLASSIFICATION CHANGED

To CONFIDENTIAL

I.N. 10,337

JUL 2 1956

By authority of NASA PA #7 Date June 2, 1959
effective date May 29, 1959.

by JBE

CLASSIFIED DOCUMENT

This material contains information affecting the National Defense of the United States within the meaning of the espionage laws, Title 18, U.S.C., Secs. 793 and 794, the transmission or revelation of which in any manner to an unauthorized person is prohibited by law.

NATIONAL ADVISORY COMMITTEE FOR AERONAUTICS

WASHINGTON

July 2, 1956

~~SECRET~~
~~CONFIDENTIAL~~

NATIONAL ADVISORY COMMITTEE FOR AERONAUTICS

RESEARCH MEMORANDUM

TESTS WITH HYDROGEN FUEL IN A SIMULATED AFTERBURNER

By W. R. Kerslake and E. E. Dangle

SUMMARY

An investigation was conducted in a 16-inch-diameter simulated afterburner using gaseous hydrogen fuel. No flameholder was used with a multipoint fuel injector. The burner length was varied from 9.5 to 38 inches. The afterburner-inlet conditions were: temperature of 1200° or 1550° F, pressure of 14 to 44 inches mercury absolute, and velocity of 300 to 780 feet per second. The measured combustion efficiency ranged from 85 to 98 percent over an equivalence-ratio range of 0.2 to 1.0. The cold-flow pressure-drop coefficient was 1.0 for the system. Spontaneous ignition was always possible at temperatures above 1200° F but was not possible below 1100° F for all pressures and velocities tested.

INTRODUCTION

Liquid hydrogen is being considered for ram-jet and turbojet fuel since the heating value per pound is approximately 2.7 times that of a hydrocarbon fuel. Although the density of liquid hydrogen is low, the high heating value per unit weight will increase the operating range considerably if the aircraft is operating at high altitudes (ref. 1). High altitudes are desirable for military aircraft since they reduce vulnerability.

For operation at high altitudes, the engine must have high thrust per unit weight. The thrust of air-breathing engines decreases rapidly with increasing altitude; thus the weight of the engine must be reduced to keep the thrust-to-weight ratio high.

Because of the high flame speed and large heat capacity of hydrogen fuel, savings in turbojet-engine weight should be possible by use of the following: (1) a compact, highly efficient primary combustor, built to operate at high-altitude conditions (ref. 2); (2) hydrogen as a heat sink for turbine cooling, permitting higher engine operating temperatures, and thus higher thrust per unit weight (refs. 1 and 3); and (3) a compact, highly efficient afterburner.

A compact efficient afterburner appears to be practical since the ram-jet-combustor development work described in reference 4 shows that hydrogen burned to 95-percent combustion efficiency in a 16-inch-long combustor at pressure, temperature, and velocity conditions of 20.9 inches mercury absolute, 618° F, and 209 feet per second, respectively. The purpose of this investigation, therefore, was to extend the ram-jet work of reference 4 to afterburner conditions. Test conditions were: inlet temperatures of 1200° or 1550° F, inlet static pressures of 14 to 44 inches mercury absolute, and velocities of 300 to 780 feet per second. The lower pressure simulated conditions in an afterburner of an advanced turbojet engine with a compressor pressure ratio of 3.1 at an altitude of 80,000 feet and a flight Mach number of 2.5. Higher altitudes were not simulated because of facility limitations.

APPARATUS

Afterburner Installation

The installation of the 16-inch-diameter simulated afterburner in the test facility is shown in figure 1. Air flow was metered by an orifice in the supply line and controlled by a butterfly valve upstream of the primary combustors. Clear gasoline was burned in four tubular turbojet combustors to heat the air from 60° to 1200° or 1550° F. The air from the four primary combustors discharged into a mixing chamber, flowed past a plug valve, and through a perforated plate into the annulus section between the 6-inch-diameter centerbody and the 16-inch-diameter outer wall. The plug valve regulated the pressure in the primary combustors, and the perforated plate was used to smooth out the velocity profile. The static-pressure-drop ratio across the mixing chamber to the annulus was 2 or more. The inlet velocity and temperature profiles, measured by rakes in the annulus, are shown in figure 2.

The combustion efficiency of the primary burner was calculated from the measured temperature rise. Corrections for radiation losses from the thermocouples were made in the efficiency calculation. This combustion efficiency varied between 90 and 104 percent, but was usually 94 to 99 percent.

The afterburner length, defined as the distance from the fuel injectors to the water-spray quench, was varied by moving the water-spray quench forward or backward. The afterburner exhaust gases and quench water spray came to equilibrium in a calorimeter, which was part water jacketed and part insulated. The resulting exhaust-gas and steam temperature was measured by thermocouple rakes before the gases flowed into the exhaust system. The exhaust system was evacuated by air ejectors.

Fuel Injection System

The hydrogen fuel was supplied in cylinders with total capacities of 420 pounds of hydrogen and a gas pressure of 2400 pounds per square inch. The fuel was taken directly from the cylinders through a pressure reducing valve, a metering orifice, and a throttling valve to the afterburner. Gas analysis of the hydrogen indicated it was more than 98 percent pure by weight.

The fuel injector consisted of five concentric rings with six supply struts. The rings were split into six equal sectors, one of which is shown in figure 3. A total of 894 injection holes, 0.038 inch in diameter, was drilled through the flattened rings. Nine-tenths of the hydrogen was sprayed cross stream, while the remainder was sprayed downstream. The fuel injectors blocked 21 percent and the centerbody 14 percent of the 16-inch-diameter cross section. The same fuel injectors were used throughout the investigation.

Engine Configurations

Configuration A is shown in figure 4(a). It consisted of a 6-inch-diameter centerbody with a tapered downstream end. The fuel injector rings were located in the annulus at the start of the taper. The water-spray quench was either 14.5 or 38.25 inches downstream of the fuel injectors.

Configuration B, shown in figure 4(b), consisted of the same centerbody as that of configuration A except that the tapered end of configuration A was replaced by a blunt end to form a sheltered piloting zone 6 inches deep. The fuel injector rings were located in the annulus, 3 inches from the end of the centerbody. The water-spray quench was either 9.5 or 16.5 inches downstream of the fuel injectors.

Configuration C, shown in figure 4(c), is configuration A with a conical exhaust nozzle. The nozzle was 12 inches long with a 0.5 contraction ratio and was water cooled. A water-cooled total-pressure rake was positioned so that the tips of 14 probes were in the plane of the nozzle exit. The distance from the fuel injectors to the total-pressure-rake tips was 20.5 inches. The water-spray quench was an additional 12 inches downstream.

METHODS AND PROCEDURE

Operating Conditions

The air flow was held constant at either of two values, approximately 54,000 or 30,000 pounds per hour. The primary combustors were set to give

an afterburner-inlet temperature of 1200° or 1550° F. An electric spark was discharged between an electrode and a fuel spray bar to ensure ignition except when the spontaneous ignition temperatures were determined. The altitude exhaust ejectors usually were set at full capacity to give the lowest pressure and highest velocity possible in the afterburner. As combustion progressed in the afterburner, the afterburner pressure increased and the velocity decreased, corresponding to the increase in heat addition.

The inlet conditions for runs 1 to 6 and 9 to 13 (table I) were selected to simulate the inlet pressure, temperature, and velocity conditions of an afterburner on an advanced turbojet engine (ref. 1) with a compressor pressure ratio of 3.1 at a flight Mach number of 2.5. The altitudes simulated by the pressures were from 58,000 to 80,000 feet.

The inlet conditions of runs 7 and 8 were selected to simulate those in an afterburner of a current turbojet engine with a compressor pressure ratio of 8.0 and a flight Mach number of 1.6. For runs 7 and 8, the altitude exhaust pressure was varied in an attempt to hold the afterburner velocity and pressure level constant for the full range of heat addition. The average velocity was 422 feet per second, and the pressure levels were 32 and 18 inches mercury absolute. The altitudes simulated by the pressures were 49,000 and 60,000 feet, respectively.

Determination of Combustion Efficiency

The heat-balance system (calorimeter) was used to obtain the combustion efficiency for all data points. The technique was similar to that first used in reference 5. In the combustion-efficiency calculation, the reaction was assumed to take place at the calorimeter-outlet temperature (approx. 800° F) to eliminate the enthalpy change of the products. Combustion efficiency was defined as the total enthalpy change of the air (1550° F or 1200° F down to 800° F), the fuel (60° up to 800° F), the quench water (60° up to 800° F), and the jacket cooling water (60° up to 120° F) divided by the lower heating value of the gaseous fuel (50,770 Btu/lb at 800° F).

When the exhaust nozzle was used (configuration C), the combustion efficiency was calculated from total-pressure measurements as well as from the heat balance. Total pressure, measured at the throat of the choked nozzle, was used with the continuity equation to calculate total temperature. The total temperature determined a theoretical afterburner equivalence ratio. The combustion efficiency was defined as the theoretical divided by the measured afterburner equivalence ratio. This definition is the same as a ratio of enthalpies if the nozzle temperature profile is uniform. The measured afterburner equivalence ratio φ_A was defined as

[redacted]

$$\varphi_A = \frac{w_f/w_a}{0.0294(1 - \varphi_p)}$$

where

w_f/w_a measured hydrogen-air ratio (where w_a is the air flow into the primary burner)

0.0294 stoichiometric fuel-air ratio for hydrogen

φ_p preheater equivalence ratio

Spontaneous Ignition

The afterburner flow was set at a desired temperature, pressure, and velocity. The hydrogen flow was then gradually increased to 0.2 of stoichiometric φ_A. Ignition was noted by either a combustor pressure rise or a temperature rise in the calorimeter.

RESULTS AND DISCUSSION

Combustion Efficiency

Configurations A and B. - The performance of configurations A and B is listed in table I and plotted in figures 5(a) and (b), respectively. It can be seen from the table and figures that variations in afterburner pressure, temperature, and velocity had negligible effect on the performance of the afterburner. Similarly, variations in the afterburner length had little effect on performance. The recirculation piloting zone included in configuration B had no effect on the combustion efficiency nor on the spontaneous-ignition temperature level of the afterburner.

The combustion-efficiency curve peaked between 0.4 and 0.7 fraction of stoichiometric at a value above 95 percent. The lean and rich ends of the efficiency curve were reasonably flat, dropping to values of approximately 87 percent at equivalence ratios of 0.2 and 1.0. Individual runs indicated slight differences in combustion efficiency with variation of inlet temperature, pressure, velocity, and burner length; but these trends were of the same order as experimental errors.

Hydrogen demonstrated no combustion limit nor instabilities over the range of variables and configurations tested.

Configuration C. - A convergent exhaust nozzle was primarily placed on the burner to measure combustion efficiency by a second independent

[redacted]

method - total-pressure measurements. The secondary reason was to determine the effect, if any, of a nozzle on the combustion or flow characteristics of the burner. The 12-inch length of the nozzle was 60 percent of the burner length.

Although the nozzle was 60 percent of the burner length, the heat-balance combustion-efficiency curve of figure 5(c) was similar to the combustion-efficiency curves measured with configurations A or B and showed no effect of the nozzle. The efficiencies calculated from the total-pressure-rake measurements were higher in the lean region and lower in the rich region than were the heat-balance efficiencies. The total-pressure efficiencies, however, were very sensitive to air leaks, incorrect air measurements, and nozzle area calibration. Due to the limited exhaust facilities the nozzle could only be operated near the critical pressure ratio; and if the nozzle were not choked, the total-pressure analysis could not be applied because of the assumption that the Mach number was unity at the nozzle exit (ref. 4).

Afterburner Pressure Losses

A total-pressure drop ΔP was measured from upstream of the fuel spray rings (station 1) to the exit of the convergent exhaust nozzle (station 3) for runs 12 and 13. Figure 6 is a plot of the total-pressure-drop coefficient $\Delta P/q_1$ against the density ratio ρ_1/ρ_3. The value of q_1 (velocity head) as well as ρ_1 (density) was calculated on the basis of the maximum cross-sectional area, a 16-inch-diameter circle. Measured values for adiabatic or cold-flow $\Delta P/q_1$ were small, about 1.0. For cold flow, $\rho_1/\rho_2 = 1.0$ and $\rho_1/\rho_3 = 1.53$. For afterburner heat addition, $\Delta P/q_1$ varied from 1.1 to 4.0.

The significant result shown in figure 6 is that the solid line drawn through the data points is almost parallel to the theoretical (dashed) line for heat addition. A parallel solid line would indicate that the heat addition took place at or near the maximum cross-sectional area. Since the data points diverge slightly from the solid line, two possibilities are indicated: (1) Burning takes place where the physical area is less than the maximum, such as the annulus or the convergent nozzle; or (2) combustion takes place in a flow region of a nonuniform velocity profile, resulting in more momentum loss in the high-velocity regions which is not completely compensated by the reduced momentum pressure loss in the low-velocity regions. For example, if all the heat release (corresponding to a ρ_1/ρ_3 of 4.0) took place in an area equal to the annulus (station 1), the theoretical $\Delta P/q_1$ due to heat addition would be 2.45 for the annulus instead of 1.73 for the 16-inch-diameter

duct. Subtracting 1.0 for cold-flow drop from the measured $\Delta P/q_1$ at ρ_1/ρ_3 of 4.0 leaves $\Delta P/q_1$ of 2.2 due to heat addition. This value could result from heat addition part way between the annulus and full 16-inch-diameter duct.

It was necessary to mass weight the measured total pressures at station 1 because of the nonuniform velocity profile. The nozzle-exit total-pressure profile was ±4 percent of the mean pressure, with lower pressures in the center and higher pressures near the walls.

Spontaneous Ignition

The afterburner-inlet-air temperature at which spontaneous ignition did or did not occur is presented in figure 7 for a range of typical pressures and velocities. The solid symbols represent spontaneous ignition at the first flow of hydrogen into the burner (φ_A of about 0.03). The tailed symbols represent delayed ignition until the fuel flow reached φ_A of about 0.2. The open symbols represent no ignition with any fuel flow up to φ_A of about 0.2. For each data point on the pressure plot, the corresponding velocity point has also been plotted.

Ignition always resulted at a temperature of 1200° F or greater but did not occur below 1100° F for all pressures and velocities tested. There was a slight decrease in the ignition temperature at the lower pressures. This decrease was consistent with the concentric-tube data of reference 6, which has been drawn as a solid line for comparison. There was no effect of velocity on the ignition temperature nor was there a difference in the data with the piloting region of configuration B over that of the tapered end of configuration A. It was likely that the ignition occurred in the disturbed air-flow region of the fuel spray rings and that the flame seated at the fuel injection port, thus eliminating the need of a flameholder.

Heat-Balance Check

The combustion efficiency measured by the calorimeter may be sensitive to the amount of quench water since it affects the (1) penetration and mixing of water jets into the air stream, (2) freezing of the reaction, (3) time to come to equilibrium in the calorimeter, and (4) heat losses through insulation. Therefore, a series of data points were taken with configuration A in which the afterburner fuel and air flow remained fixed while the amount of quench water was varied to give different outlet equilibrium temperatures.

[redacted]

The results are included in figure 8 for four different afterburner flow conditions. All four conditions gave acceptible combustion efficiencies in the normal operating range (700° to 800° F) of the calorimeter. Three of the conditions resulted in a flat combustion-efficiency curve even for the extreme range of calorimeter temperatures. The explanation for the curve at the fourth afterburner condition was that the system was not designed for a wide range of calorimeter temperatures at this lowest air and fuel-flow condition. The percentage error of flow measurements at this condition was greater; and certain assumptions, such as negligible heat loss in the insulated part of the calorimeter, were no longer valid.

SUMMARY OF RESULTS

The following results were obtained from combustion of hydrogen fuel in a 16-inch-diameter simulated afterburner for inlet-air temperatures of 1200° or 1550° F, pressures of 14 to 44 inches of mercury absolute, velocities of 300 to 780 feet per second, and burner lengths of 9.5 to 38 inches.

1. Hydrogen was burned with a maximum efficiency of 98 percent in a 14.5-inch-length and an efficiency of 95 percent in a 9.5-inch-length afterburner. The efficiency curve was reasonably flat, dropping to 87 percent at 0.2 or 1.0 fraction of stoichiometric.

2. The resulting combustion efficiency was not significantly changed with the test range of temperature, pressure, velocity, or burner length.

3. Hydrogen demonstrated no combustion limit or instabilities over the range of variables and configurations tested. Also, no flameholder was required, as the flame seated on the fuel spray rings.

4. The pressure-drop coefficient across the fuel spray rings and exhaust nozzle was about 1.0 without combustion. With combustion, the pressure-drop coefficient increased by an amount only slightly greater than the theoretical value due to heat addition.

5. Hydrogen fuel spontaneously ignited at inlet-air temperatures above 1200° F but did not ignite below 1100° F for the entire range of pressures and velocities tested.

Lewis Flight Propulsion Laboratory
National Advisory Committee for Aeronautics
Cleveland, Ohio, April 16, 1956

[redacted]

REFERENCES

1. Lewis Flight Propulsion Laboratory: NACA Conference on Aircraft Propulsion Systems, 1955.

2. Friedman, Robert, Norgren, Carl T., and Jones, Robert E.: Performance of a Short Turbojet Combustor with Hydrogen Fuel in a Quarter-Annulus Duct and Comparison with Performance in a Full-Scale Engine. NACA RM E56D16, 1956.

3. Silverstein, Abe, and Hall, Edon W.: Liquid Hydrogen as a Jet Fuel for High-Altitude Aircraft. NACA RM E55C28a, 1955.

4. Dangle, E. E., and Kerslake, William R.: Experimental Evaluation of Gaseous Hydrogen Fuel in a 16-Inch-Diameter Ram-Jet Engine. NACA RM E55J18, 1955.

5. Cervenka, A. J., and Miller, R. C.: Effect of Inlet-Air Parameters on Combustion Limit and Flame Length in 8-Inch-Diameter Ram-Jet Combustion Chamber. NACA RM E8C09, 1948.

6. Coward, H. F.: Ignition Temperatures of Gases. "Concentric Tube" Experiments of (the late) Harold Baily Dixon. Jour. Chem. Soc. (London), pt. II, July-Dec. 1934, pp. 1382-1406.

[redacted]

TABLE I. - PERFORMANCE OF HYDROGEN IN 16-INCH-DIAMETER AFTERBURNER

Afterburner equivalence ratio	Combustion efficiency, percent	Afterburner-inlet			Air flow, lb/hr	Hydrogen flow, lb/hr	Preheater	
		Pressure, in. Hg abs	Temperature, °F	Velocity, ft/sec			Gasoline flow, lb/hr	Combustion efficiency, percent
		Run 1, configuration A						
0.277	85.0	21.3	1237	636	5.60×10^4	322	817	96
.437	97.9	24.8	1237	547	5.23	507	895	96
.658	93.9	28.3	1241	481	5.25	766	895	97
.787	90.0	31.5	1246	448	5.25	915	895	96
.861	89.7	30.5	1246	433	5.25	1001	895	96
Run 2, configuration A								
0.198	89.4	13.5	1212	547	2.88×10^4	127	515	90
.383	96.2	15.7	1227	484	2.95	251	515	92
.476	95.3	16.9	1204	442	2.93	313	515	90
.721	92.9	19.9	1229	383	2.95	473	515	93
.951	86.5	18.7	1221	408	2.97	631	510	94
.965	86.5	18.8	1230	408	2.97	637	515	94
Run 3, configuration A								
0.217	87.1	21.0	1561	785	5.32×10^4	229	1180	97
.385	92.1	23.2	1567	712	5.32	406	1180	98
.540	95.7	25.3	1583	658	5.31	565	1180	99
.688	94.3	27.6	1577	602	5.32	722	1180	99
Run 4, configuration A								
0.251	90.0	13.9	1555	658	2.95×10^4	147	680	94
.359	89.5	16.2	1571	565	2.93	208	680	94
.517	93.7	15.5	1578	594	2.95	300	680	95
.673	93.3	16.7	1585	551	2.93	388	680	95
.830	92.7	18.2	1590	509	2.95	480	680	96
.987	87.9	19.2	1599	483	2.93	566	680	96
Run 5, configuration A								
0.221	94.8	21.3	1192	632	5.35×10^4	266	826	101
.531	103.9	26.3	1199	512	5.32	632	826	102
.698	99.1	28.9	1205	467	5.32	829	817	102
.824	91.8	30.4	1205	444	5.32	979	812	103
1.040	86.0	32.9	1205	410	5.31	1231	800	104
Run 6, configuration A								
0.498	97.1	17.7	1182	427	3.01×10^4	337	475	100
.694	94.7	17.1	1181	448	3.06	478	480	100
.854	90.5	18.1	1215	432	3.06	581	508	98
1.033	86.4	19.5	1210	399	3.06	702	493	101

TABLE I. - Continued. PERFORMANCE OF HYDROGEN IN 16-INCH-DIAMETER AFTERBURNER

Afterburner equivalence ratio	Combustion efficiency, percent	Afterburner-inlet			Air flow, lb/hr	Hydrogen flow, lb/hr	Preheater	
		Pressure, in. Hg abs	Temperature, °F	Velocity, ft/sec			Gasoline flow, lb/hr	Combustion efficiency, percent
Run 7, configuration B								
0.187	93.5	32.5	1195	436	5.62×10^4	235	911	98
.281	98.0	32.3	1205	442	5.62	351	911	99
.416	98.2	32.5	1210	440	5.61	519	914	100
.672	94.9	31.8	1220	446	5.54	827	914	99
.873	91.7	34.4	1214	393	5.30	1036	865	97
1.162	78.1	34.4	1268	395	5.16	1321	865	100
Run 8, configuration B								
0.308	92.6	17.5	1221	442	3.01×10^4	208	523	93
.420	93.1	18.4	1245	424	3.01	279	525	95
.484	94.6	18.0	1221	430	3.02	326	513	96
.764	94.2	18.4	1279	417	2.89	482	523	94
1.140	82.8	19.6	1271	394	2.91	727	523	94
1.400	69.6	22.2	1183	360	3.19	1009	508	98
Run 9, configuration B								
0.282	95.5	22.0	1508	715	5.22×10^4	298	1107	98
.488	94.4	25.4	1515	621	5.22	515	1107	98
.637	94.9	27.5	1520	575	5.21	670	1107	98
.769	92.5	29.0	1525	547	5.21	807	1107	99
.965	85.6	31.0	1523	511	5.21	1013	1107	99
1.132	77.8	32.4	1531	491	5.21	1185	1107	99
Run 10, configuration B								
0.184	91.8	14.0	1513	631	2.91×10^4	108	637	96
.375	91.8	16.8	1515	525	2.91	220	637	96
.540	92.4	16.2	1520	546	2.91	316	637	96
.767	92.1	16.7	1524	530	2.91	448	637	96
.955	86.2	17.6	1535	505	2.90	556	637	97
1.09	82.6	19.5	1538	456	2.90	633	637	97
Run 11, configuration B								
0.203	92.6	21.7	1331	664	5.26×10^4	230	986	95
.342	98.8	23.2	1330	621	5.26	388	979	95

TABLE I. - Concluded. PERFORMANCE OF HYDROGEN IN 16-INCH-DIAMETER AFTERBURNER

Afterburner equivalence ratio	Combustion efficiency, percent		Afterburner-inlet			Air flow, lb/hr	Hydrogen flow, lb/hr	Preheater	
	Heat balance	Total pressure	Pressure, in. Hg abs	Temperature, °F	Velocity, ft/sec			Gasoline flow, lb/hr	Combustion efficiency, percent
Run 12, configuration C									
0.171	89.0	101.8	29.8	1204	451	5.30×10^4	203	831	101
.249	90.3	98.3	32.0	1243	435	5.36	297	840	101
.321	94.0	100.0	33.6	1202	400	5.30	381	831	101
.375	95.7	93.4	35.2	1245	395	5.36	446	840	102
.396	96.8	91.5	35.4	1225	388	5.35	472	840	103
.515	96.7	92.9	37.4	1202	360	5.30	612	822	102
.635	98.2	86.0	39.3	1245	353	5.34	752	826	102
.708	95.4	80.7	40.2	1202	334	5.28	840	819	101
.841	93.3	85.5	41.9	1202	320	5.29	996	822	102
.967	87.7	77.8	43.5	1209	312	5.24	1136	816	102
1.127	81.7	78.8	43.5	1212	302	5.24	1321	816	102
Run 13, configuration C									
1.155	72.2	99.2	17.5	1209	440	3.06×10^4	106	508	96
.277	86.6	101.9	19.4	1196	401	3.07	190	496	97
.399	88.1	90.9	21.2	1192	369	3.09	277	496	98
.557	92.7	93.8	23.2	1191	336	3.08	386	496	97
.690	95.9	86.9	24.1	1179	322	3.10	483	496	97
.783	93.5	88.9	25.1	1201	312	3.07	541	494	98
.949	89.5	85.3	26.2	1200	301	3.09	658	494	98

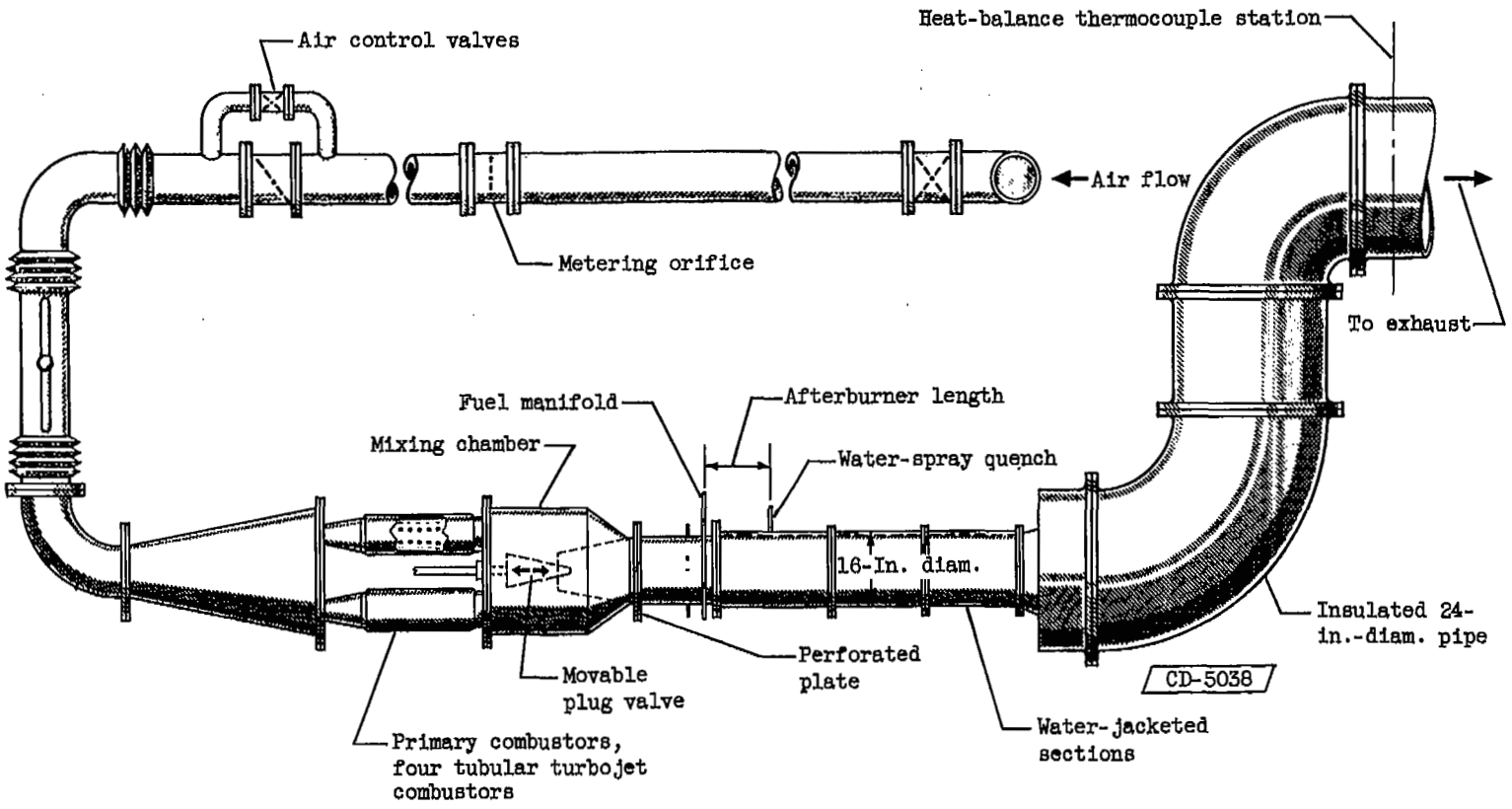

Figure 1. - Installation of 16-inch-diameter afterburner in connected-pipe facility.

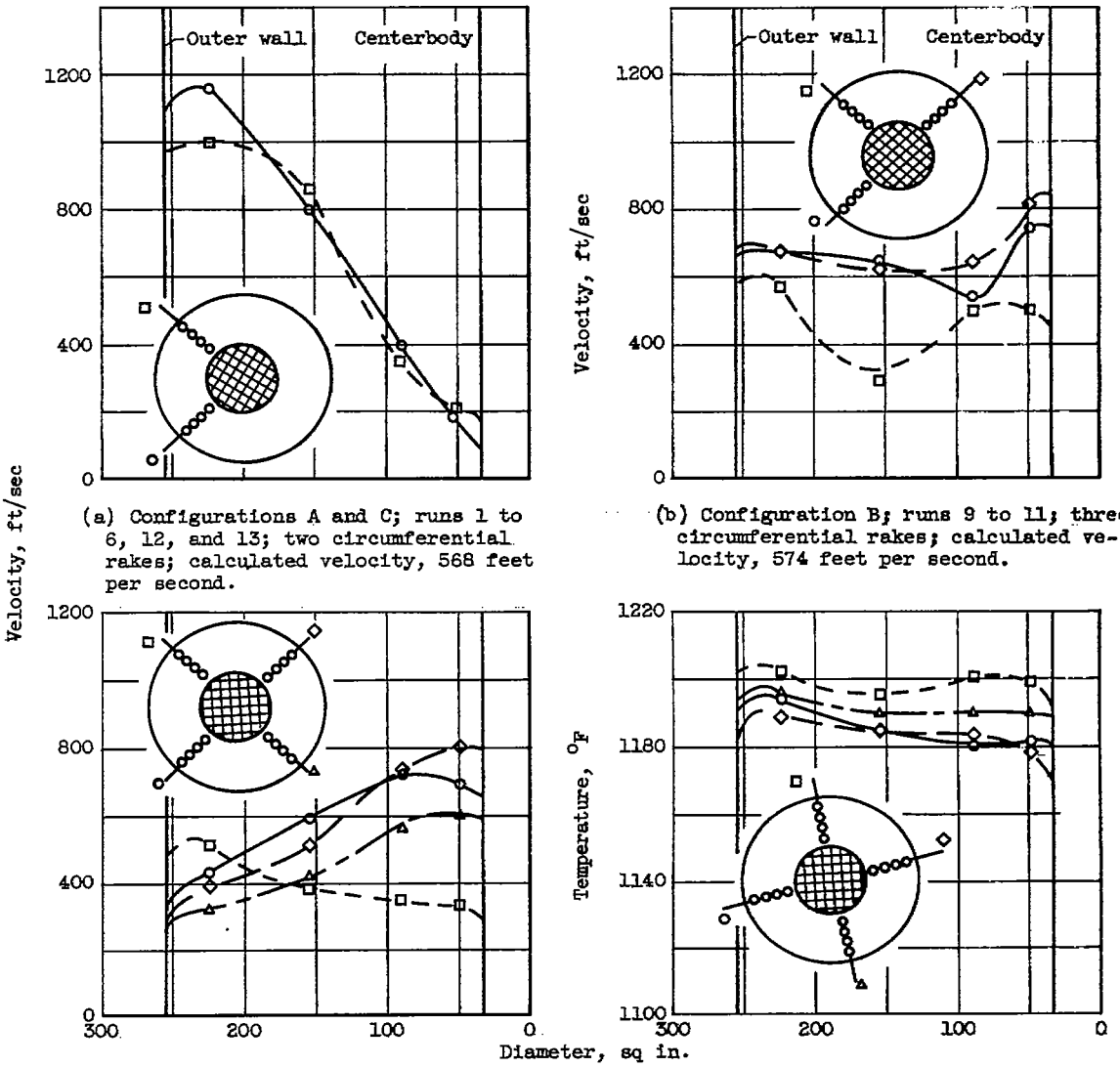

(a) Configurations A and C; runs 1 to 6, 12, and 13; two circumferential rakes; calculated velocity, 568 feet per second.

(b) Configuration B; runs 9 to 11; three circumferential rakes; calculated velocity, 574 feet per second.

(c) Configuration B; runs 7 and 8; four circumferential rakes; calculated velocity, 430 feet per second.

(d) Configurations A, B, or C; four circumferential rakes; uncorrected for radiation.

Figure 2. - Typical inlet velocity and temperature profiles at annulus section of 15-inch-diameter simulated afterburner.

4091

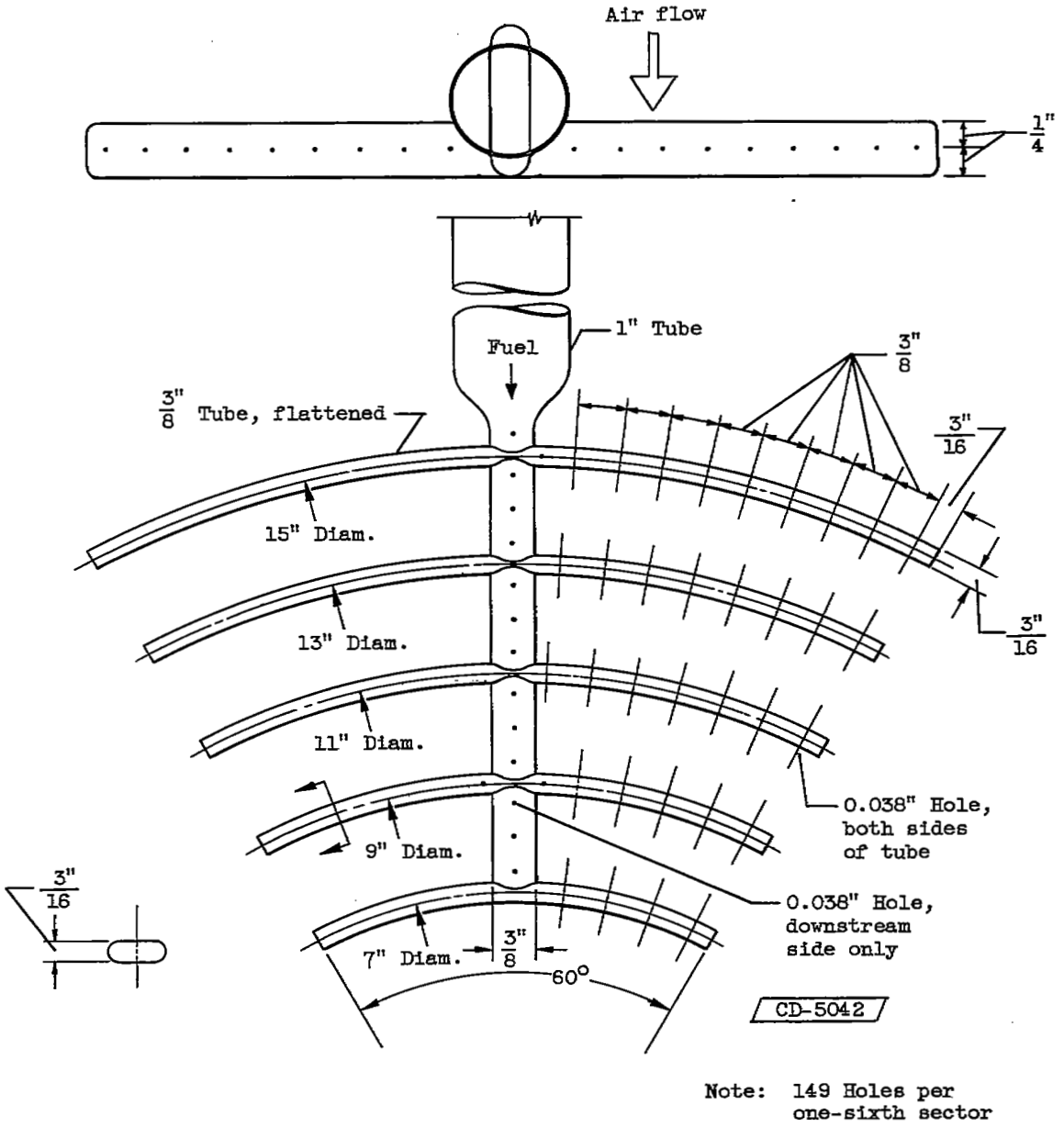

Note: 149 Holes per one-sixth sector

Figure 3. - Details of fuel spray rings, one-sixth sector only.

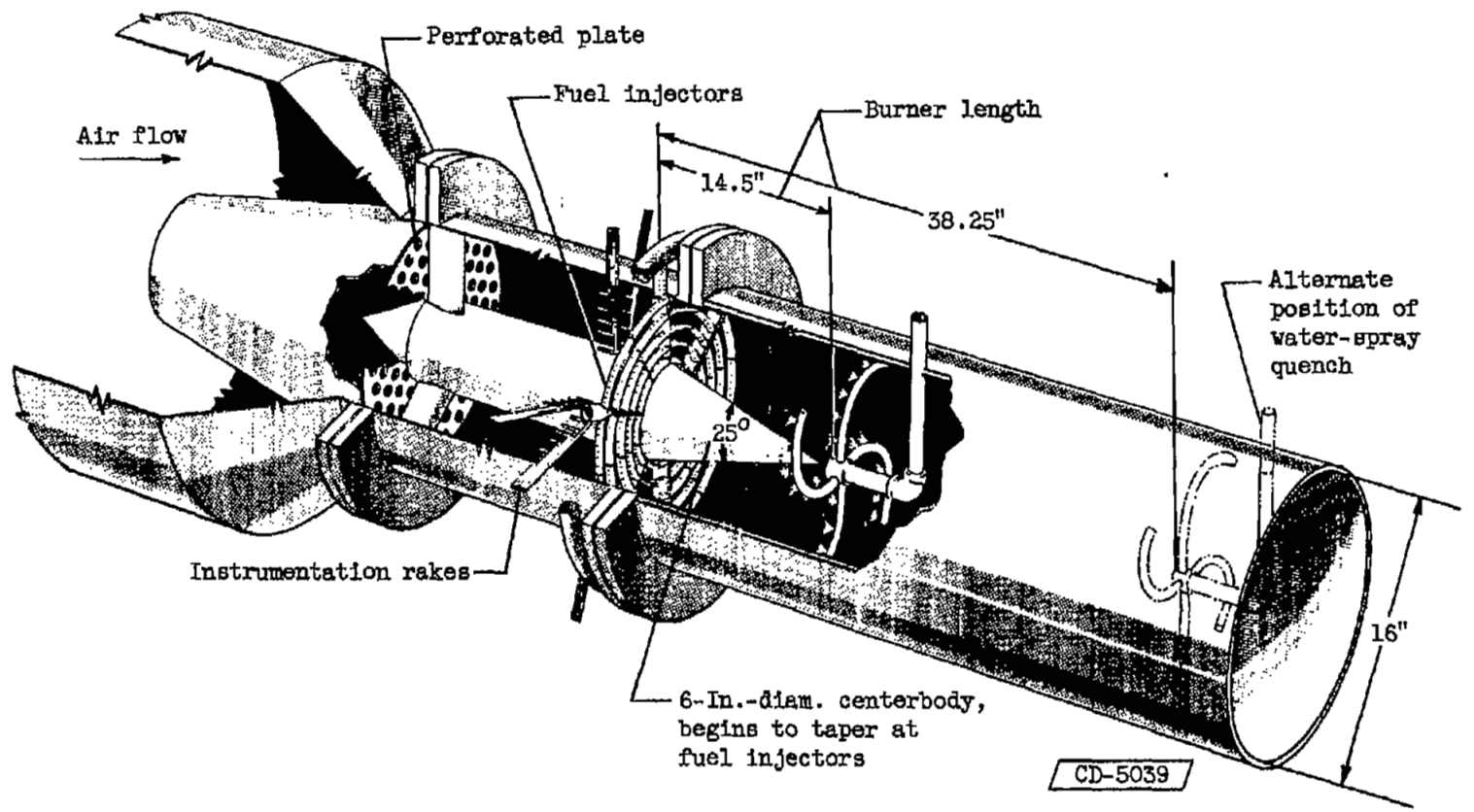

(a) Configuration A.

Figure 4. - Details of afterburner configurations.

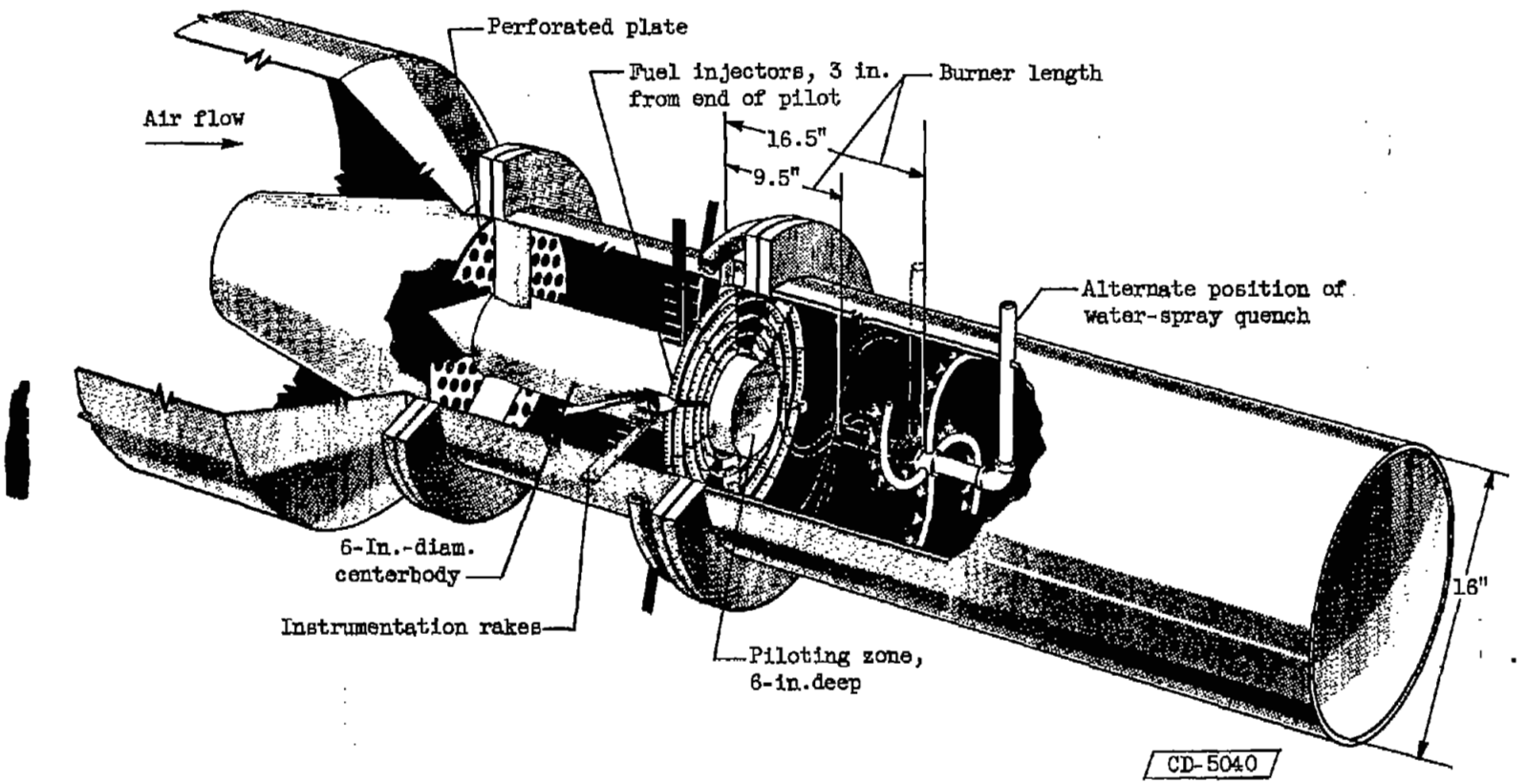

(b) Configuration B.

Figure 4. - Continued. Details of afterburner configurations.

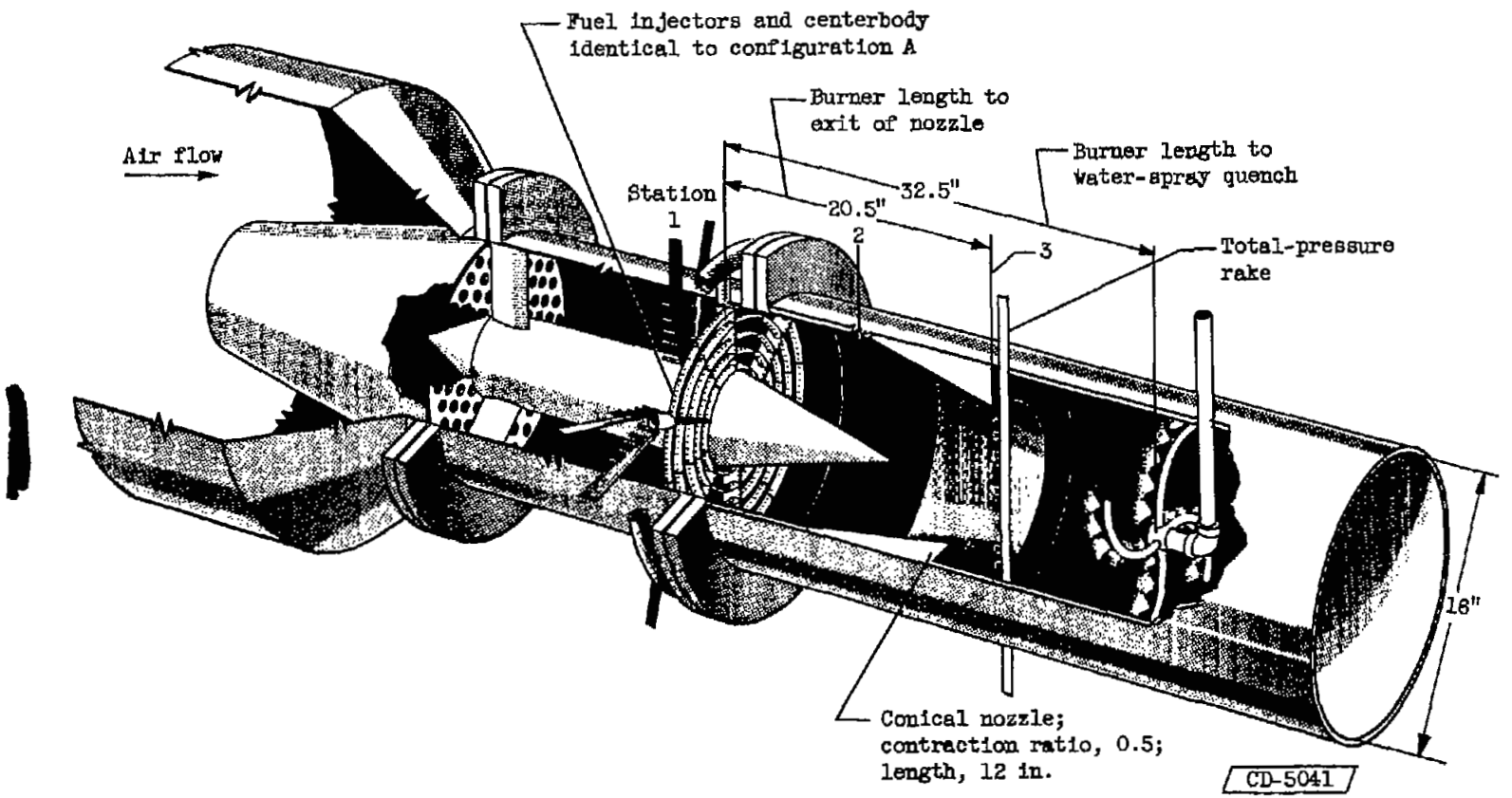

(c) Configuration C.

Figure 4. - Concluded. Details of afterburner configurations.

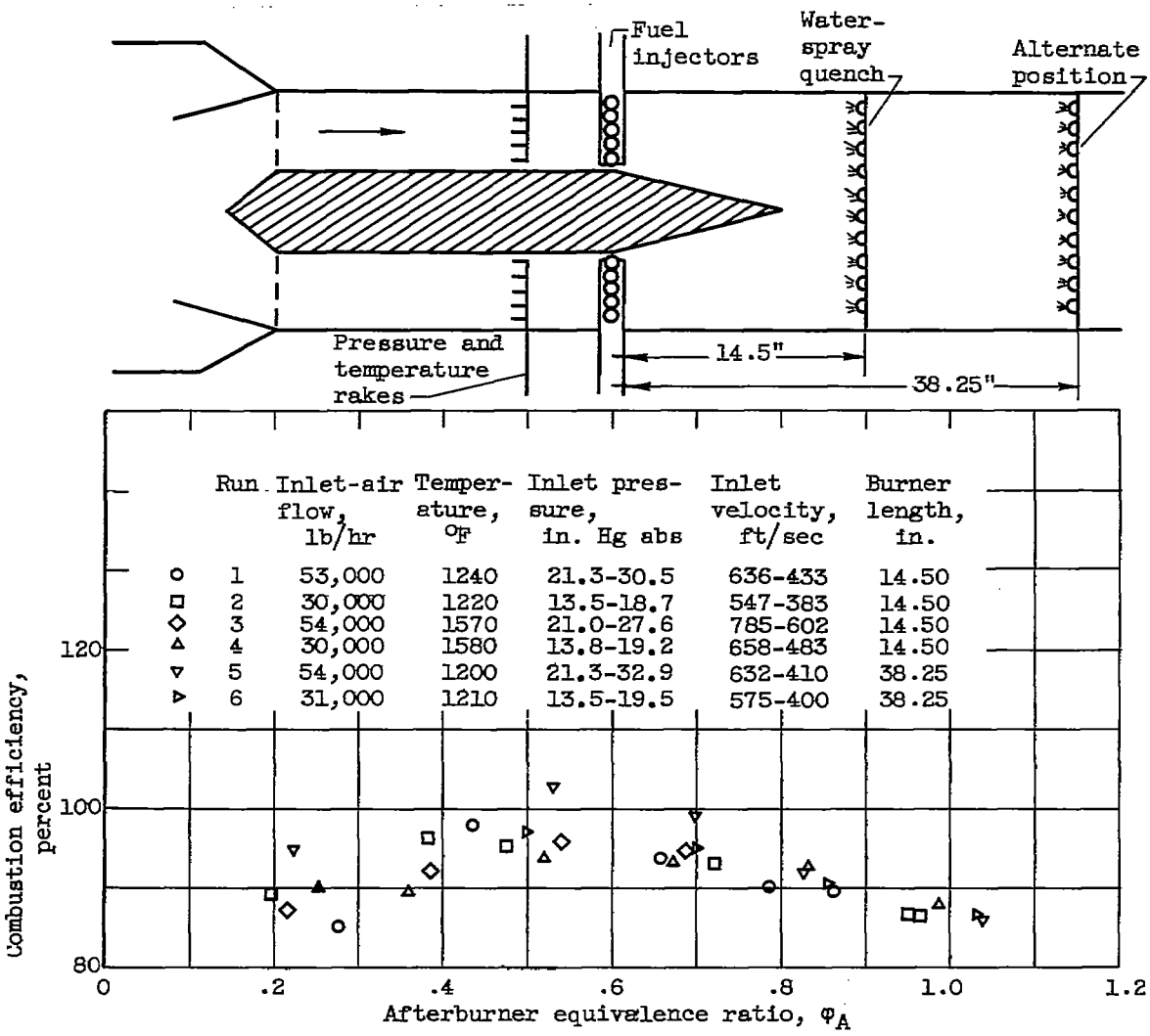

(a) Configuration A (tapered centerbody).

Figure 5. - Combustion efficiencies.

[redacted]

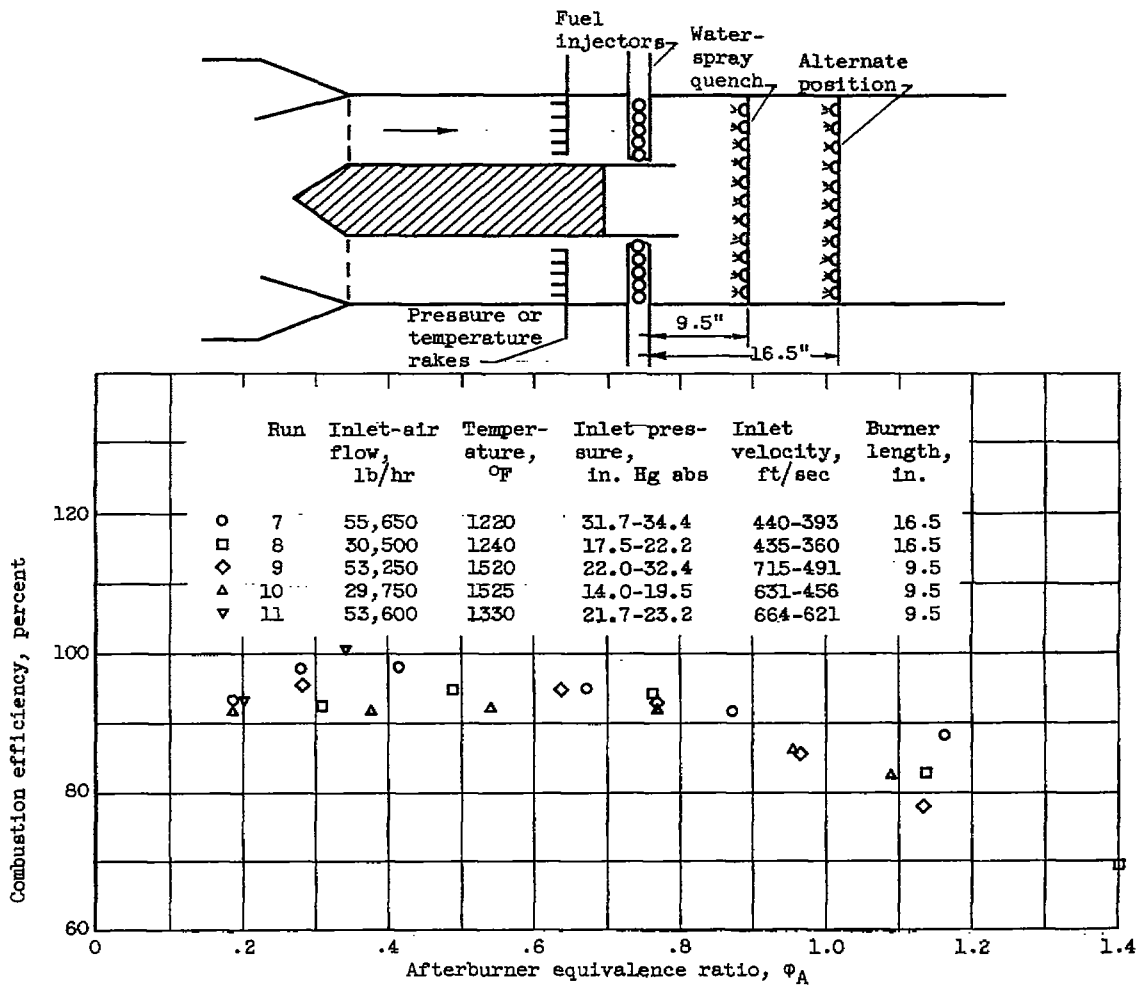

(b) Configuration B (blunt-end centerbody).

Figure 5. - Continued. Combustion efficiencies.

[redacted]

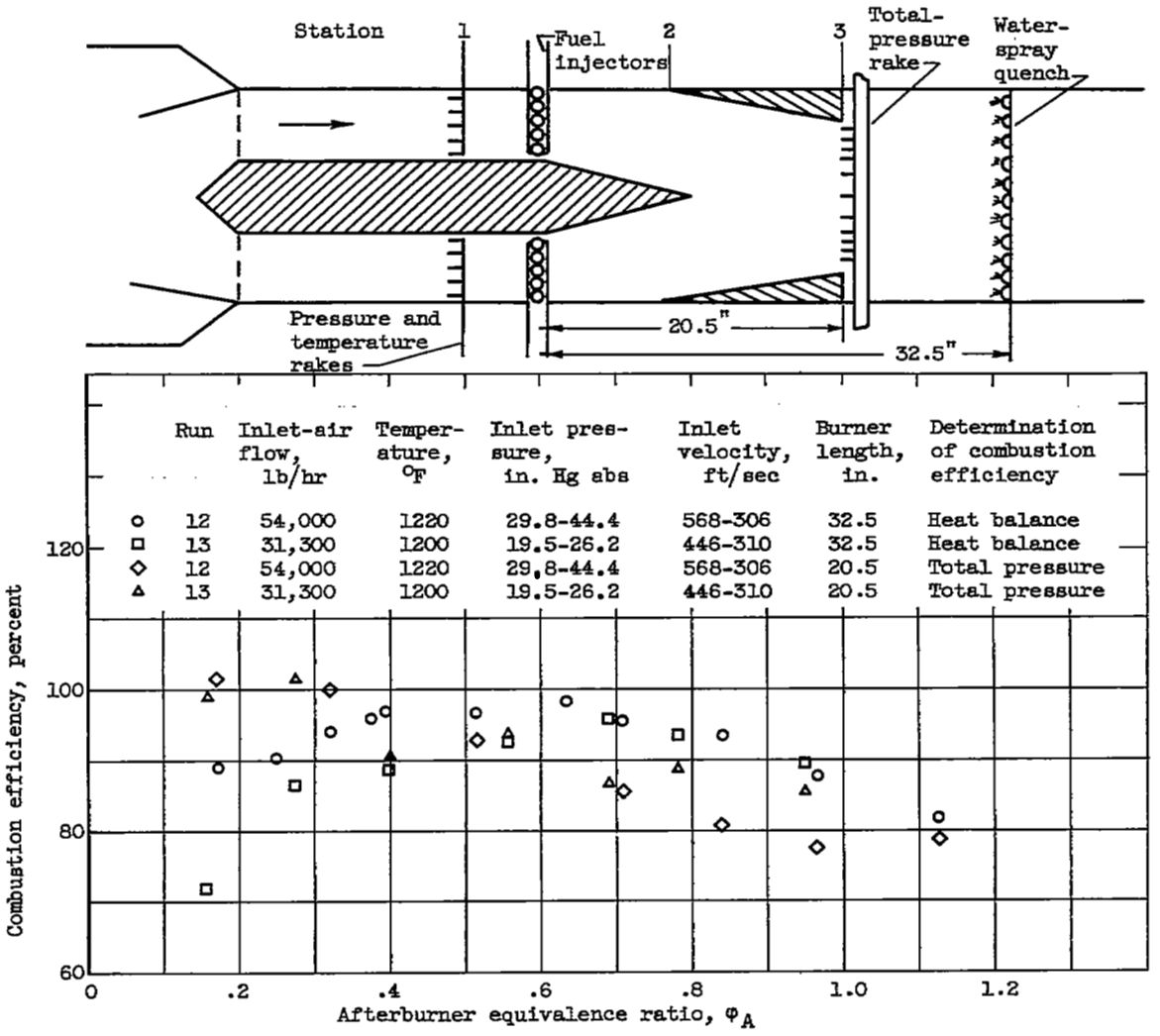

(c) Configuration C (exhaust nozzle).

Figure 5. - Concluded. Combustion efficiencies.

[redacted]

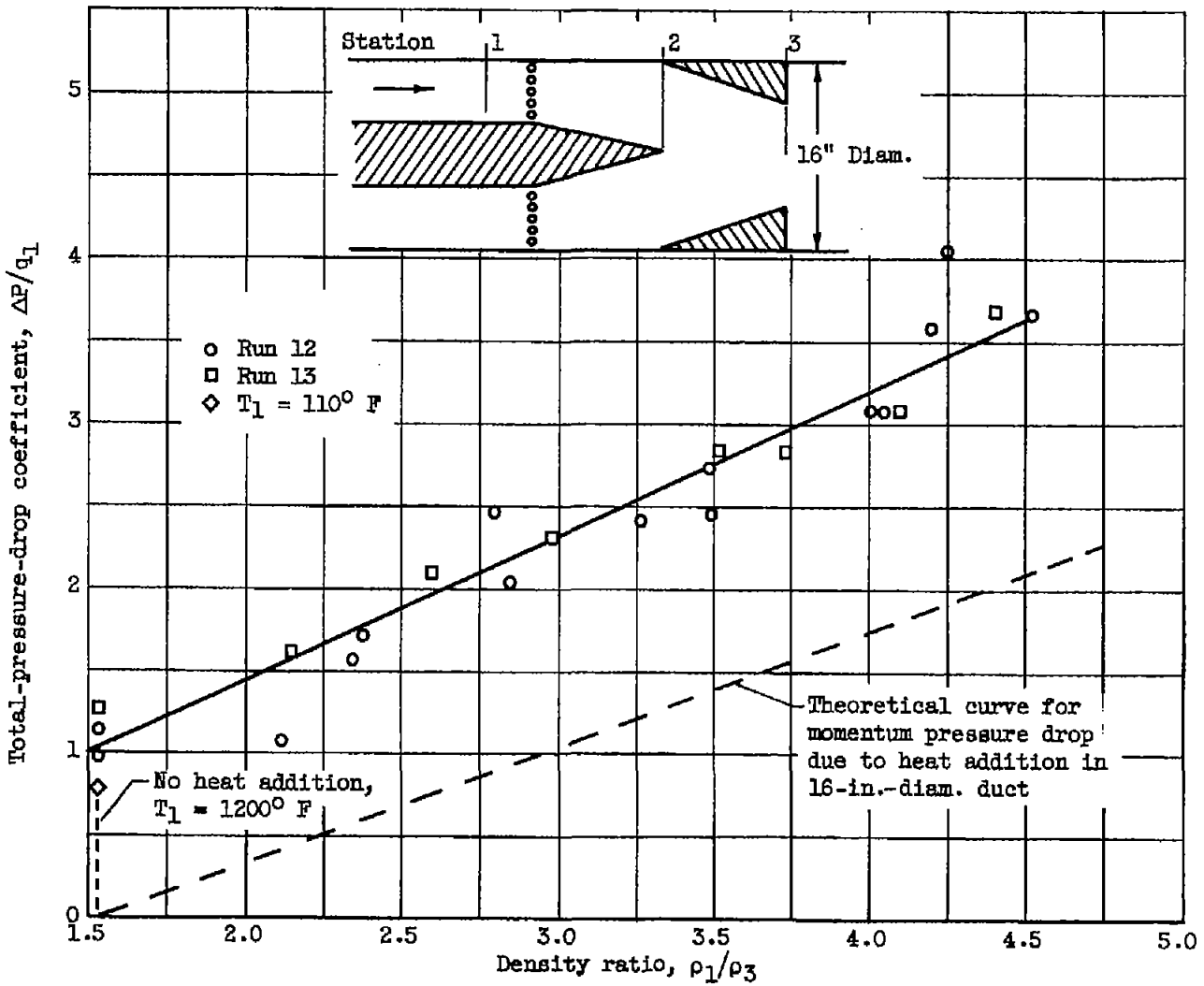

Figure 6. - Total-pressure-drop coefficient for various heat additions in afterburner for configuration C. $\Delta P = P_1 - P_3$; q_1, velocity head, basis 16-inch diameter.

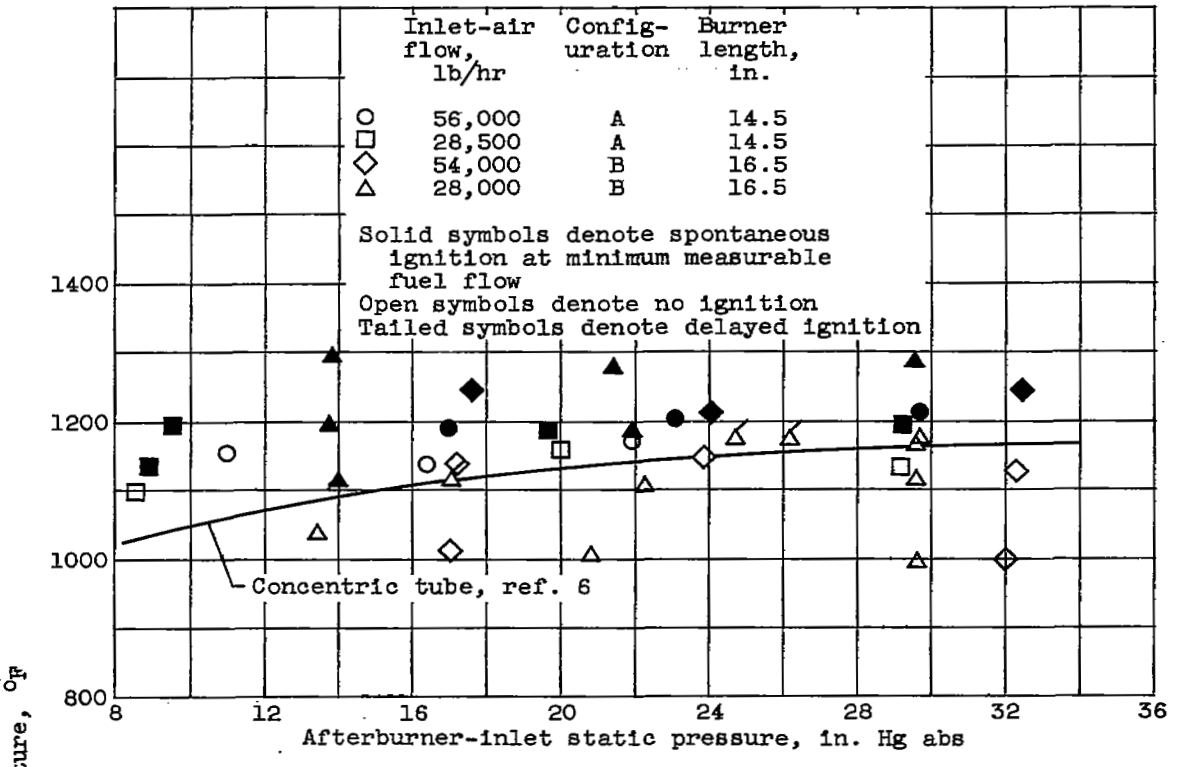

(a) Pressure.

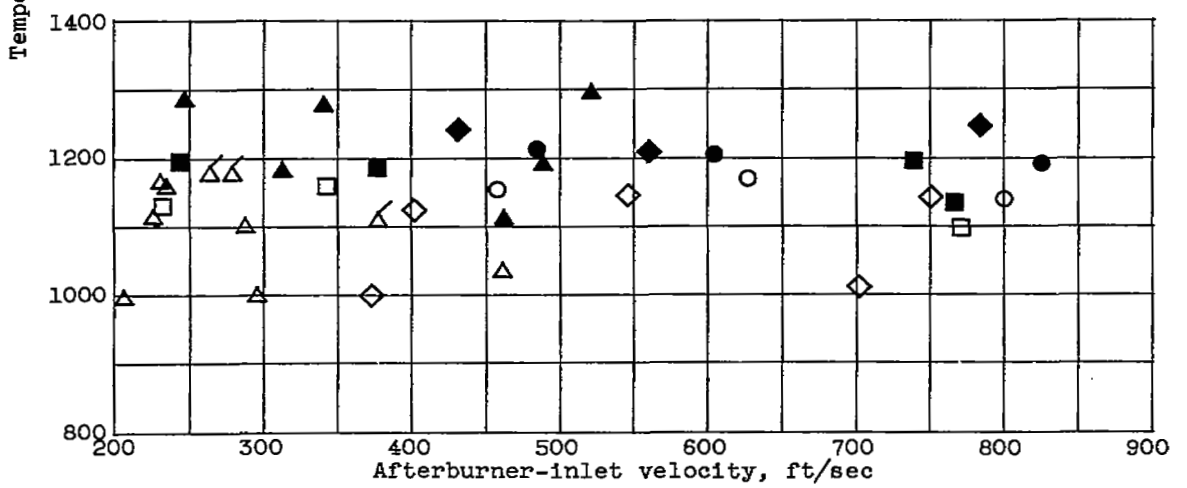

(b) Velocity.

Figure 7. - Spontaneous ignition temperature of hydrogen fuel at various air-flow conditions in 16-inch-diameter simulated afterburner.

[redacted]

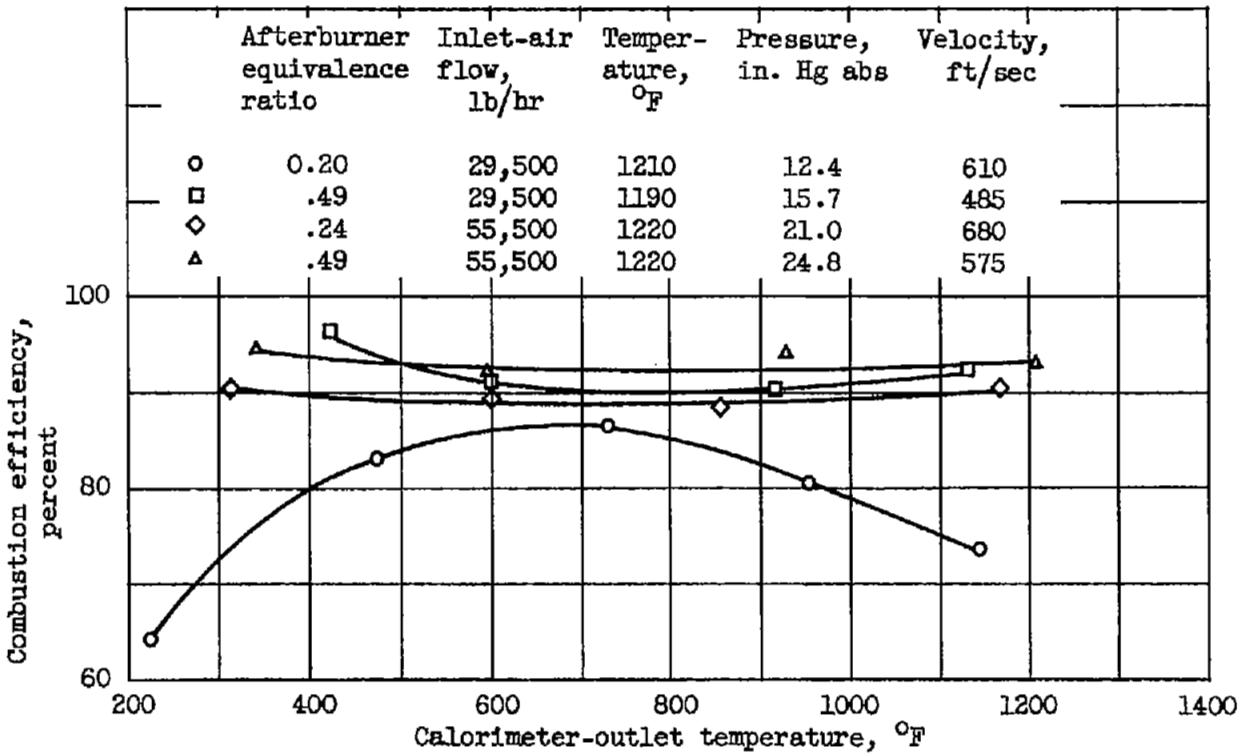

Figure 8. - Effect of variable quench-water flow on measured combustion efficiency. Configuration A (burner length, 14.5 in.).

[redacted]

[redacted]